Intelligent Bearing Anomaly Detection for Industrial Internet of Things Based on Auto-Encoder Wasserstein Generative Adversarial Network

Ruonan Liu, *Member, IEEE*, Dong Xiao, Di Lin, *Member, IEEE*, and Weidong Zhang, *Senior Member, IEEE*

***Abstract*—Bearing anomaly detection plays a crucial role in modern industries as most rotating machinery faults are attributed to faulty bearings. However, acquiring fault samples in industry is a time-consuming and expensive process. To address this issue, this article presents an integrated unsupervised learning method named autoencoder Wasserstein generative adversarial network (AE-AnoWGAN). AE-AnoWGAN is capable of detecting abnormal bearings and performing anomaly localization without the need for labeled data. In this approach, industrial data is initially processed using continuous wavelet transform to convert it into time-frequency representations (TFRs). These TFRs are then fed into the integrated AE-AnoWGAN for training. AE-AnoWGAN consists of multiple encoder–decoder and discriminator pairs, which are randomly paired and trained using adversarial training. The encoder maps the TFRs to a latent space, and the pretrained generator acts as the decoder to generate reconstructed TFRs. During the testing phase, the model calculates anomaly scores for the input TFRs. Experimental evaluations were conducted using the PU bearing data set and IMS bearing data set. Comparative results demonstrate that the proposed AE-AnoWGAN method outperforms existing approaches in terms of anomaly detection accuracy. Moreover, the method exhibits high-anomaly detection efficiency, making it suitable for real-time monitoring applications. Furthermore, this method provides practical value by enabling anomaly localization and bearing degradation estimation of TFRs.**

***Index Terms*—Anomaly detection, deep learning, fault diagnosis, Wasserstein generative adversarial network (WGAN).**

Acronyms and Abbreviations

G_d	Decoder in autoencoder–discriminator pair.
G_e	Encoder in autoencoder–discriminator pair.
L_a	Adversarial loss.
L_d	Discriminative loss.
L_r	Reconstruction loss.
$\mathcal{S}(\mathbf{x})$	Anomaly score.
$\mathbf{x}$	Time-frequency representations (TFRs).
$\mathbf{z}$	Latent space representation.
D	Discriminators in generative adversarial network (GAN).
G	Generators in generative adversarial network (GAN).

Manuscript received 12 December 2023; revised 15 January 2024; accepted 19 January 2024. Date of publication 2 February 2024; date of current version 26 June 2024. This work was supported in part by the National Natural Science Foundation of China under Grant 62206199 and Grant U2141234; in part by the Tianjin Applied Basic Research Project under Grant 22JCQNJC00410; in part by the Young Elite Scientist Sponsorship Program under Grant YESS20220409; in part by the Alexander von Humboldt Foundation under Grant 1226831; and in part by the State Key Laboratory of Reliability and Intelligence of Electrical Equipment under Grant EERI-KF2022001.
(Corresponding author: Di Lin.)

Ruonan Liu is with the Department of Automation, Shanghai Jiao Tong University, Shanghai 200240, China (e-mail: liuruonan04@163.com).

Dong Xiao and Di Lin are with the College of Intelligence and Computing, Tianjin University, Tianjin 300350, China (e-mail: 3020244106@tju.edu.cn; ande.lin1988@gmail.com).

Weidong Zhang is with the Department of Automation, Shanghai Jiao Tong University, Shanghai 200240, China, and also with the School of Information and Communication Engineering, Hainan University, Haikou 570228, Hainan, China (e-mail: wdzhang@sjtu.edu.cn).

Digital Object Identifier 10.1109/JIOT.2024.3358871

I. Introduction

RECENTLY, the popularization of Industrial Internet of Things (IIoT) technology has accelerated the arrival of the industrial big data era, which means that more and more industrial data can be recorded and used for data-driven fault detection [1], [2], [3], [4]. As one of the critical components in industrial systems, bearings have been widely used in encompassing motors, wind turbines, gearboxes and automobiles [5], [6]. Many instances of equipment degradation or failure can be attributed to bearing failures. Consequently, the condition monitoring of bearings has emerged as a focal point of research in recent years [7], [8]. This approach not only enhances the security of industrial systems but also offers substantial economic savings.

In recent literature, data-driven fault diagnosis methods, especially deep learning-based intelligent fault diagnosis methods, have led to a series of breakthroughs due to its powerful ability that can directly learns the high-level features from massive raw data. For now, autoencoders [9], convolutional neural networks (CNNs) [10], recurrent neural networks (RNNs) [11], deep adversarial capsule network [12], deep ensemble capsule network [13], WavCapsNet [14], weight-shared capsule network [15], et al., have been proposed to solve the complex diagnosis tasks for rotating machines. However, the annotation of fault data is a time-consuming and needs comprehensive domain knowledge. We cannot guarantee to get enough data under every condition to train a deep network. Therefore, many research works have been proposed to solve the few-shot fault diagnosis problem with class-imbalance data set [16], which can be generally divided into three aspects: 1) data augmentation; 2) model construction;

and 3) optimization algorithm. The data augmentation algorithms can enlarge data set and solve the few-shot problem from data level, which mainly including simulation data augmentation [17], [18], affine transform, GAN, and so on. Then, the model construction, including transfer learning [16], multitask learning [19], continual learning [20], etc., is also important for class-imbalance data analyze and has shown great advantages for few-shot fault diagnosis. Third, as for model optimization, meta-learning is the most widely used algorithm, which can learn the general parameters of the network based on historical tasks, thus converge quickly via a few samples [21]. Additionally, the trained model is constrained to anomalies that have been predefined and well-known, making it challenging, if not impossible, to identify rare and previously unknown faults.

Unsupervised learning serves as an effective tool for identifying rare fault anomalies, offering a solution that does not rely on labeled data and playing a more and more important role in industrial big data analysis and other IoT systems. Qi and Luo [22] reviewed the recent progresses on unsupervised learning methods for big data. Shang et al. [23] proposed a feature-based implicit irregularity detection for unsupervised homecare IoT system. Guo et al. [24] developed a gated recurrent unit-based Gaussian mixture variational autoencoder scheme for smart cities IoT systems. Leveraging its ability to learn high-dimensional distributions of real engineering data, generative adversarial network (GAN) and adversarial training frameworks [25] have been successfully employed in bearing anomaly detection. One notable example is AnoGAN, which was initially proposed for anomaly detection utilizing GANs [26]. AnoGAN initially employs a standard GAN to train on normal samples and learns a mapping from the latent space z to real samples x: $G(\mathbf{z}) = \mathbf{z} \mapsto \mathbf{x}$. Subsequently, it maps the TFRs [27] to be tested back to the latent space. The model is trained using normal samples, allowing it to learn the manifold $\mathcal{X}$ of normal sample TFRs. As the generator is trained to generate normal TFR samples, when an abnormal TFR needs to be encoded in the test set, the reconstruction of this abnormal TFR becomes an outlier. Thus, an abnormality arises between the input TFR and the reconstructed TFR. While AnoGAN demonstrates promising anomaly detection performance, it has been observed to suffer from training instability issues in practical applications.

To address this problem in AnoGAN, the Wasserstein distance [28] is proposed, which provides a smoother training process, thereby enhancing stability. In WGAN, the discriminator quantifies the Wasserstein distance between the generated data and the real data distribution, without distinguishing between real and generated samples. Rather than using weight clipping as a means to enforce the Lipschitz constraint, an improved training procedure called WGAN-GP [29] is introduced. In WGAN-GP, the discriminator outputs the gradient norm directly, which is constrained by the discriminator input. Training generative adversarial networks poses challenges due to the need for optimizing multiple deep neural networks within a min-max problem. Optimization often leads to stability issues. Additionally, inadequate regularization of the neural network can result in mode collapse. Recent research [30] has demonstrated that utilizing multiple generators and discriminators can effectively address these challenges. Multiple studies have employed the use of multiple discriminators to ensure stable gradients for the generator, thereby enhancing the smoothness of the training process.

Several studies have explored the application of GANs in anomaly detection, including models, such as AnoGAN, EGBAD, GANomaly, and Skip-GANomaly. These models commonly employ an encoder–decoder architecture as the generator. The generator's decoder produces synthetic samples that are either reconstructions of real samples or entirely new samples. The discriminator's role is to distinguish between synthetic samples and normal samples, thereby acquiring the ability to identify anomalies within the data. The anomaly score is typically computed by evaluating the sample's reconstruction and its internal representation in the discriminator. These models have demonstrated strong performance across various detection tasks.

Although AnoGAN and its variants can generate TFRs by learning the data distribution and successfully detect abnormal TFRs, they still have the following drawbacks: 1) the training of these models is prone to instability and mode collapse [31] and 2) the low-detection efficiency of these models is a critical limitation in practical anomaly detection for industrial systems. To address these limitations, this article proposes an ensemble of auto-encoder Wasserstein GAN(AE-AnoWGAN). AE-AnoWGAN replaces the reconstruction process by learning the mapping from TFRs to the latent space using an autoencoder. This approach significantly enhances efficiency and stability without compromising effectiveness. In AE-AnoWGAN, the WGAN is trained using normal samples, an autoencoder receives feedback from multiple discriminators, while a discriminator evaluates "training samples" generated by multiple generators. The anomaly score is computed as the average of scores obtained from all encoder–decoder discriminator pairs. The interactive learning of multiple generators and discriminators enhances the modeling of the normal data distribution, leading to improved accuracy in anomaly detection.

The main contributions of the proposed method are summarized as follows.

1) An ensemble of multiple autoencoders and discriminators is employed in the proposed method to effectively model the distribution of normal data. The embedding of generator–discriminator pairs can help the model to capture data patterns via multiple generators and provide diversity to synthetic samples, thereby enhancing both the accuracy of anomaly detection and the stability of the training process.
2) A discriminator-guided approach is proposed and incorporated into AE-AnoWGAN for reconstructing TFRs. Then, based on the integration of adversarial loss, reconstruction loss and discrimination loss, an anomaly score is proposed in this article to quantify the anomalies of the TFRs.

II. Proposed Method

The complete anomaly detection framework involves the following steps: 1) ensemble adversarial training; 2) training the ensembled AE-AnoWGAN; and 3) calculating anomaly scores on the test set to determine the abnormality of the current bearing.

Before performing adversarial training on WGAN [32], the TFRs of normal and abnormal data sets are generated using wavelet transform. During adversarial training, each generator is paired with each discriminator. The generator is then evaluated by each discriminator, which receives synthetic samples from each generator, resulting in an adversarial loss. The WGAN is adversarially trained using normal TFRs, which yields a preliminary trained generator and discriminator. During the training process of AE-AnoWGAN, we establish an autoencoder–discriminator pair, where the encoder maps TFRs to the latent space, and the previously trained generator serves as the decoder to generate reconstructed TFRs. The discriminator is employed to identify the reconstructed samples, and the reconstruction loss and discrimination loss are calculated using multiple autoencoder–discriminator pairs. The integration of generator–discriminator pairs can help the model to capture data patterns via multiple generators and provide diversity to synthetic samples. Multiple generators may also have a larger joint support S than a single generator. Therefore, the integrated model can achieve better performance than a single model. In the training process of AE-AnoWGAN, the Encoder is trained to generate an inverse mapping from the image input and then use the Decoder to decode for image reconstruction. Then, the condition of the image is normal or abnormal can be determined by evaluating the quality of reconstruction because the abnormality of the image determines the quality of the reconstruction. And a discriminator is used to distinguish normal and abnormal samples from the final hidden layer. Ultimately, our anomaly score can be calculated by the integration of adversarial loss, reconstruction loss and discrimination loss, and the size of these losses determines the size of the anomaly score. A detailed description of the method is provided below. Fig. 1 depicts the framework of AE-AnoWGAN, showcasing its architectural design.

A. Ensemble Adversarial Training

For the training of GAN and encoders, normal time-frequency diagrams $\mathbf{x} = \mathbf{x}_{k,n} \in \mathcal{X}$ are used to convert vibration signals from industrial data sets into TFRs via wavelet transform [33]. In the formula, $\mathbf{x}_{k,n}$ is the TFR of a certain n device parts in the whole normal data set, and is cut into K parts to extract an TFR block of size $s \times s$, with $k = 1, 2, \ldots, K$. N industrial devices are converted to time-frequency and uncut pictures, with $n = 1, 2, \ldots, N$. During the training step, Only unlabeled normal TFRs are used.

During the test step, the data set with class M faults is converted into TFRs as the test set, Then, the proposed method in the training set is used to obtain a TFR of size $s \times s$. The normal TFRs are also mixed in the test set to determine whether the model can correctly distinguish between normal TFRs and anomaly TFRs.

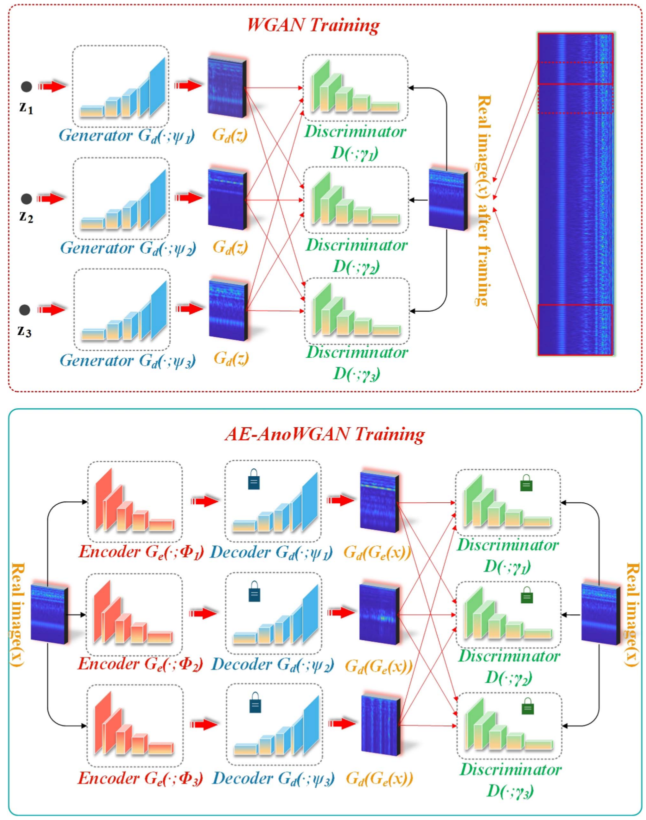

Fig. 1. Framework of the proposed AE-AnoWGAN for bearing anomaly detection. The red dotted box corresponds to the WGAN training process, which involves parameter training for both the generator (G) and discriminator (D). The blue section represents the training process of AE-AnoWGAN. In this process, we employ an autoencoder–discriminator pair. The encoder maps TFRs to a latent space, while the pretrained generator acts as the decoder to generate reconstructed TFRs. The discriminator is utilized to distinguish the reconstructed samples. Multiple pairs of autoencoders and discriminators are employed to calculate the reconstruction loss and identification loss for anomaly detection.

Learning normal data distribution by generating adversarial networks. Generally, a GAN consists of two adversarial modules, a generator G and a discriminator D [34]. The generator G learns the distribution on the data $\mathbf{x}$ by mapping the sample $\mathbf{z}$ to $G(\mathbf{z})$. The sample $\mathbf{z}$ is a 1-D vector of uniformly distributed input noise sampled from the latent space $\mathcal{Z}$, which will be mapped to a 2-D TFR in the time-frequency space manifold $\mathcal{X}$ that is filled with normal examples.

During the GAN training, the parameters of generator G and discriminator D are optimized simultaneously [35]. By sampling the input noise from the latent space $\mathbf{z}$, the generator trains the TFR of the output data $\mathcal{X}$ to be as close as possible to the normal TFR of the real input in order to trick the discriminator. Thus, a training distribution TFR that captures normal changes can be generated via the generator G, and the fitting degree of the generated TFR to the normal TFR can be estimated via the discriminator D [36]. The loss function of WGAN L_{wgan} is

$$L_{\text{wgan}}(\mathbf{x}) = D(\mathbf{x}) - D(G_d(\mathbf{z})). \tag{1}$$

$D(\mathbf{x})$ represents the discrimination process performed by the discriminator, $G_d(\mathbf{z})$ represents the generation of samples using input $\mathbf{z}$, and $G_d(\mathbf{z})$ serves as the decoder in AE-AnoWGAN after training.

In the adversarial training phase, each generator is paired with each discriminator. The discriminators evaluate the generators by receiving synthetic samples from each generator. The training objectives of the ensembled WGAN are as follows:

$$\max \sum_{i=1}^{I} \sum_{j=1}^{J} L_{\text{wgan}}^{ij}. \tag{2}$$

L_{wgan}^{ij} represents the loss value between each generator–discriminator pair (i, j), and the discriminator is trained by maximizing the cumulative adversarial losses. The framework consists of I generators and J discriminators.

B. Training the Ensembled AE-AnoWGAN

AE-AnoWGAN comprises multiple autoencoder–discriminator pairs, with the autoencoder serving as the generator. We define I generators, $\mathcal{G} = \{(G_e(\cdot; \Phi_i), G_d(\cdot; \Psi_i)) : i = 1, \ldots, I\}$, and J discriminators $\mathcal{D} = \{D(\cdot; \gamma_j) : j = 1, \ldots, J\}$.

After WGAN training, the generator has learned the mapping $G_d(\mathbf{z}) = \mathbf{z} \mapsto \mathbf{x}$ from the latent space representation $\mathbf{z}$ to the normal TFR $\mathbf{x}$. But GANs cannot automatically generate an inverse mapping $G_e(\mathbf{x}) = \mathbf{x} \mapsto \mathbf{z}$. Therefore, a deep autoencoder network $\mathcal{G}$ is trained in this article to learn the map function $G_e(\mathbf{x}) = \mathbf{x} \mapsto \mathbf{z}$.

1) Reconstruction Loss: During the training process, the real TFR is initially processed by the trainable encoder G_e to map it to the corresponding latent encoding $\mathbf{z}$. Subsequently, the decoder G_d is employed to reconstruct the TFR from the mapped latent space.

Our objective is to minimize the discrepancy between the input sample $\mathbf{x}$ and its reconstructed counterpart $\mathbf{x}$. To achieve this, we employ the mean square error (MSE) as the loss metric, measuring the difference between the two samples. The reconstructed sample $\mathbf{x}$ is represented by $G_d(G_e(\mathbf{x}))$. This component of the loss is referred to as the reconstruction loss $L_r(\mathbf{x})$. It quantifies the disparity between the reconstructed samples and the original samples, which is inherited from the encoder–decoder architecture

$$L_r(\mathbf{x}) = \frac{\|G_d(G_e(\mathbf{x})) - \mathbf{x}\|^2}{m} \tag{3}$$

where m is the number of the TFR pixels, and $\|\cdot\|^2$ is the sum of squared pixel-wise residuals.

2) Discriminative Loss: The residuals in the feature space, which are estimated by the discriminator, play a vital role in the training objectives of the encoder as they are crucial for identifying anomalous TFRs. Previous research has indicated that the hidden vector h, obtained from the final hidden layer of the discriminator $D(\cdot; \gamma)$, is often informative for discriminating between normal and abnormal samples. Denote $\mathbf{m} = f_D(\mathbf{x}; \gamma)$ as the hidden vector of $\mathbf{x}$ in $D(\cdot; \gamma)$, then the discriminative loss $L_d(\mathbf{x})$ based on $\mathbf{m}$ is

$$L_d(\mathbf{x}) = \frac{\mathcal{K} \cdot \|f_D(G_d(G_e(\mathbf{x}))) - f_D(\mathbf{x})\|^2}{m_d} \tag{4}$$

where m_d is the dimension of the middle layer features representation. $\mathcal{K}$ is the weight size.

3) Adversarial Loss: During the adversarial training process, the adversarial loss remains consistent with that of the WGAN process. However, in this case, the adversarial loss L_a is computed between the encoder–decoder and the discriminator

$$L_a(\mathbf{x}) = D(\mathbf{x}) - D(G_d(G_e(\mathbf{x}))). \tag{5}$$

4) Ensemble Loss: During AE-AnoWGAN training, we pair each generator with every discriminator. Each discriminator then evaluates the generator and receives synthetic samples generated by each generator. With multiple pairs of generators and discriminators, both adversarial and discriminative losses are computed for each generator–discriminator pair. We denote the loss $L_a^{(ij)}$ and $L_d^{(ij)}$ between each generator–discriminator pair (i, j)

$$L_a^{(ij)} = L_a(\mathbf{x}; \Phi_i, \Psi_i, \gamma_j) \tag{6}$$

$$L_d^{(ij)} = L_d(\mathbf{x}; \Phi_i, \Psi_i, \gamma_j). \tag{7}$$

Let us denote the reconstruction loss L_r^i for a specific generator i as follows:

$$L_r^i = L_r(\mathbf{x}; \Phi_i, \Psi_i). \tag{8}$$

Finally, the generator is trained by minimizing the cumulative sum of all losses. The training objectives can be summarized as follows:

$$\min \sum_{i=1}^{I} \sum_{j=1}^{J} \beta_1 L_a^{(ij)} + \beta_2 L_r^i + \beta_3 L_d^{(ij)}. \tag{9}$$

During each training iteration, we update a single generator–discriminator pair instead of updating all generators and discriminators simultaneously. Specifically, we randomly select one generator and one discriminator, and then compute the loss using a randomly selected batch of training data. Algorithm 1 provides an overview of the AE-AnoWGAN training process.

C. Anomaly Detection

Once the training of AE-AnoWGAN is finished, we develop an anomaly score to assess the abnormality of input TFRs. The anomaly score, denoted as $\mathcal{S}(\mathbf{x})$ for a new instance $\mathbf{x}'$, is computed based on the loss function employed during the training phase

$$\mathcal{S}(\mathbf{x}') = L_r(\mathbf{x}') + L_d(\mathbf{x}'). \tag{10}$$

The anomaly score of the ensemble $\mathcal{A}(\mathbf{x}')$ for a new instance $\mathbf{x}'$ is the average of anomaly scores from multiple generators and discriminators

$$\mathcal{A}(\mathbf{x}') = \frac{1}{IJ} \sum_{i=1}^{I} \sum_{j=1}^{J} S(\mathbf{x}'; \Phi_i, \Psi_i, \gamma_j). \tag{11}$$

Taking the average of anomaly scores helps mitigate the influence of false positive anomaly detections.

When an anomalous TFR is provided as input, the reconstructed TFR exhibits significant deviations. Consequently,

Algorithm 1 AE-AnoWGAN Training

Input: Training set $X = \{x_{k,n}\}$ with $k = 1, \ldots, K$ and $n = 1, \ldots, N$
Output: Trained generators $\{(G_e(\cdot; \Phi_i), G_d(\cdot; \Psi_i))\}_{i=1}^{I}$ and discriminators $\{D(\cdot; \gamma_j)\}_{j=1}^{J}$

Initialize parameters for $(\Phi_i, \Psi_i)_{i=1}^{I}$ and $(\gamma)_{j=1}^{J}$
$t \leftarrow 0$
while Components do not **do**
  converge and $t <$ max_*iter*
  for i from 1 to I **do**
    for j from 1 to J **do**
      Sample a minibatch X^t from X
      Compute the adversarial loss $L_a^{(ij)}$
      Update $D(\cdot; \gamma_j) : \gamma_j \leftarrow \gamma_j + \nabla_{\gamma_j} L_a^{(ij)}$
      $\mathcal{L}^{(ij)} = \beta_1 L_a^{(ij)} + \beta_2 L_r^i + \beta_3 L_d^{(ij)}$
      Update $G_e(\cdot; \Phi_i) : \Phi_i \leftarrow \Phi_i - \nabla_{\Phi_i} \mathcal{L}^{(ij)}$
      Update $G_d(\cdot; \Psi_i) : \Psi_i \leftarrow \Psi_i - \nabla_{\Psi_i} \mathcal{L}^{(ij)}$
      $t \leftarrow t + 1$
    end for
  end for
end while

Algorithm 2 Anomaly Detection

Input: Test set $X' = \{x'_{k,n}\}$ with $k = 1, \ldots, K$ and $n = 1, \ldots, N$
Input: Trained generators $\{(G_e(\cdot; \Phi_i), G_d(\cdot; \Psi_i))\}_{i=1}^{I}$ and discriminators $\{D(\cdot; \gamma_j)\}_{j=1}^{J}$
Output: Anomaly Score $\mathcal{A}(x')$

for x' in X' **do**
  for i from 1 to I **do**
    for j from 1 to J **do**
      Reconstructed value $x'_r \leftarrow G_d(G_e(x'))$
      Compute reconstruction loss $L_r(x')$
      Compute discriminator loss $L_d(x')$
      Compute single anomaly score $\mathcal{S}(x')$
      Update $\mathcal{A}(x') \leftarrow \mathcal{A}(x') + \mathcal{S}(x')$
    end for
  end for
end for

the anomalies yield higher anomaly scores. Generally, the capability to reconstruct similar TFRs is inversely proportional to the degree of anomaly. Thus, the absolute value of the pixel residual, denoted as $\dot{\mathcal{A}}_R(\mathbf{x})$, is defined as follows for pixel-level positions:

$$\dot{\mathcal{A}}_R(\mathbf{x}) = |G_d(G_e(\mathbf{x})) - \mathbf{x}|. \tag{12}$$

The anomaly scores and anomaly positioning can be utilized to detect the degree and location of anomalies in TFRs. Through the interactive learning of multiple generators and discriminators, the distribution of normal data can be more effectively modeled, leading to enhanced accuracy in anomaly detection. Algorithm 2 outlines the anomaly detection process and the acquisition of anomaly scores.

III. Case Study

To assess the effectiveness of the proposed anomaly detection method, we conduct separate analyses on the PU bearing data set and the IMS bearing data set. The PU bearing data set is the real vibration signals of prefabricated faults and natural failure, and the IMS data sets are run-to-failure data sets, which can illustrate the effectiveness of the proposed method in real engineering.

To begin with, The original data set is the time-series vibration signals collected via acceleration sensors. After the experiments finished, we can get a time-series vibration vector data set. Then, the data set is transformed from the time domain to the time-frequency domain using continuous wavelet transform (CWT) [37], which can combine the information in time domain and frequency domain together, thus supports the neural networks get more accuracy results. This transformation enables us to obtain the TFR of both normal and abnormal bearings under various operating conditions. Subsequently, the WGAN model is trained using the TFRs of normal bearings to enable the generator to produce realistic TFRs resembling normal bearings. During the training process of AE-AnoWGAN, each generator interacts with each discriminator, receiving feedback from them. The encoder is utilized to map the TFRs into a latent space, and the previously trained generator serves as the decoder to generate reconstructed TFRs. By employing an ensemble of multiple generators and discriminators, a better modeling of the distribution of normal data is achieved, leading to improved anomaly detection.

During the testing phase, inputting samples into the model yields anomaly scores for each sample, facilitating the assessment of the severity of anomalies. Simultaneously, pixel-level anomaly localization is performed. In the comparative experiment, several anomaly detection methods are employed to analyze the identical data set for comparison. These methods include GANomaly [38], a GAN-based anomaly detection approach, as well as other methods, such as FastFlow [39], PADIM [40], STFPM [41], and reverse distillation [42].

The algorithm is implemented by Python based on GPU NVIDIA RTX 2060 6GB and CPU AMD Ryzen 7 4800H.The platform is Pytorch1.0. For the WGAN training, the GPU memory cost is 5722 Mb.

A. Case I—PU Bearings Data Set

1) Data Description: The PU bearing data set used in this study was provided by Lessmeier [43] for the purpose of condition monitoring and diagnosis of bearings, which is contributed by Paderborn University and collected current signals and vibration signals of rolling bearings under different conditions, including artificially damaged, naturally damaged, and healthy state. The artificial damages are manually caused by manual electric engraving and electric discharge machining drilling. The data set consists of 32 bearings of type 6203, which were subjected to various tests. Among them, there are 12 artificially damaged bearings, 14 naturally failed bearings that have passed accelerated life tests, and 6 healthy bearings.

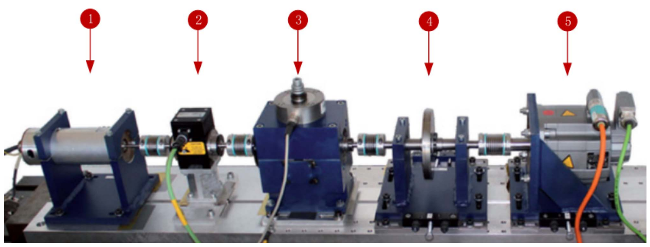

Fig. 2. Mechanical setup of the test rig: (1) test motor; (2) measuring shaft; (3) bearing module; (4) flywheel; and (5) load motor.

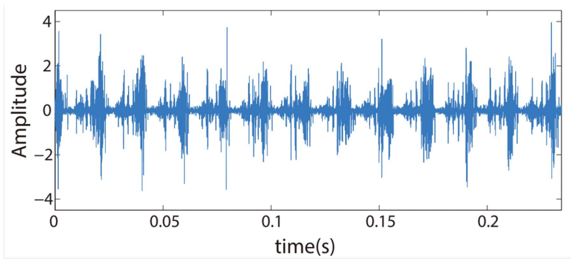

Fig. 3. Visualization of vibration signal from PU data set.

These bearings were tested under four different operating conditions.

For artificially simulated faults, three processing modes were considered. The bearings with natural failures were obtained through accelerated run-to-failure tests. Subsequently, all bearings were mounted on a modular test bench to ensure uniform testing conditions. During the experiment, the current signals, vibration signals, and three parameters (radial force, load torque, and oil temperature) were collected.

Each bearing was affixed onto a standardized modular test rig to ensure consistent testing conditions. The experimental setup utilized to gather the PU bearing data set is illustrated in Fig. 2. The visualization of the vibration signal is shown in Fig. 3.

2) Data Preprocessing: The wavelet transform was employed to process the industrial signals, facilitating the transformation of the signals into time-frequency representations (TFRs) [44]. The Morlet wavelet was chosen as the wavelet basis due to its suitability for analyzing nonstationary signals with both time and frequency localization properties. Its complex Gaussian shape and adjustable width make it well-suited for capturing transient features in industrial signals [45].

The scale parameter, also known as the window length, was set to 64 samples. This choice was based on a tradeoff between time and frequency resolution. A shorter window provides better time resolution but sacrifices frequency resolution, while a longer window increases frequency resolution but reduces time resolution. The selected scale parameter strikes a balance between the two, allowing for an adequate representation of both time and frequency characteristics.

The PU data set incorporates the K001 and KA01 bearing data sets, representing vibration data from a healthy bearing and a faulty bearing with artificially induced grooves via electrical discharge machining, respectively. The data is partitioned into frames with a size of $f = 1024$. Using the aforementioned wavelet transform, TFRs of the preprocessed PU data sets are obtained, encompassing TFRs of both healthy and faulty states. Consequently, 3920 TFRs with dimensions of 256×256 pixels are obtained for the healthy state, while 3871 TFRs with the same dimensions are obtained for the faulty state. To train the AE-AnoWGAN, 70% of the normal TFRs are utilized as the training set, while the remaining 30% of healthy TFRs and all faulty TFRs are randomly designated as the test set for anomaly detection. The number of total samples, training samples and test samples are listed in Table I.

TABLE I
SAMPLES OF THE TWO CASES

Dataset	All Samples	Training Samples	Test Samples
PU Dataset	7791	2744	5047
IMS Dataset	6245	3003	3242

TABLE II
PARAMETER SETTINGS IN COMPARATIVE EXPERIMENTS

	FastFlow	PADIM	STFPM	RD	GANomaly
learning_rate	0.00001	0.001	0.4	0.005	0.0002
batch_size	32	32	32	16	32
weight_decay	0.00001	-	0.0001	-	-
momentum	-	0.8	0.9	-	-
beta1	-	-	-	0.5	0.5
beta2	-	-	-	0.99	0.999

*RD is the abbreviation of Reverse Distillation

3) Experimental Setup: During the WGAN training, a ResNet is trained with gradient penalty (WGAN-GP), where the generator and the discriminator were implemented as convolutional decoder and encoder, respectively. Each of them is comprised with four residual blocks. Throughout the process, the size of filters is set to be 3×3. In the discriminator, layer normalization is used. The hyperparameters of WGAN are set as $batch\_size = 32$, $iterations = 100$ and $learning\_rate = 0.0002$.

During encoder training, the encoder map is constrained within $(-1\sigma, +1\sigma)$ of the standard normal distribution by applying a tanh activation function to the encoder output. The training parameters of the encoder are the same as those of WGAN. The backbone of FastFlow, PADIM, and STFPM is Resnet18, and the backbone of Reverse Distillation is wide_resnet50_2. Other parameter settings are shown in Table II.

4) WGAN Training: the WGAN is employed to generate realistic TFRs from a latent space, mapping from the latent space to the TFR domain. Fig. 4(a) and (b), depict the generated TFR and the original TFR, respectively. As framed in yellow, it can be found two main components in the raw TFR in Fig. 4(b): 1) the 5800-Hz periodic harmonic vibration component and 2) the harmonic vibration component between 3000 to 4000 Hz, which matches with the knowledge of healthy bearings. And in the generated TFR in Fig. 4(a), the two periodic harmonic vibration components have all been generated well. The structural similarity index (SSIM) is utilized as a metric to assess the similarity between the two TFRs. The closer to 1 of SSIM, the closer between the generated samples and original samples, the better the model is. The average SSIM value computed for the generated TFR

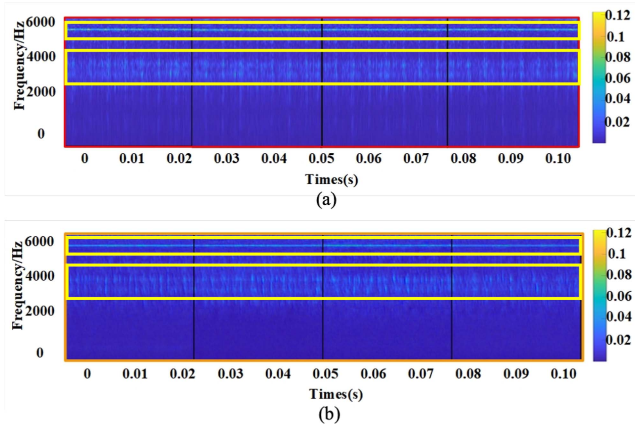

Fig. 4. (a) Generated TFR of healthy bearing and (b) raw TFR input of healthy bearing.

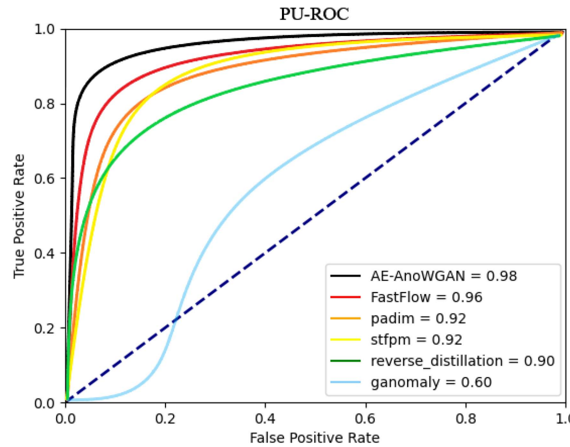

Fig. 5. ROC curve and AUC value of the analyzed results for the PU data set are presented. It is evident that AE-AnoWGAN exhibits the highest accuracy rate among the methods evaluated.

and the original TFR is 0.93, indicating a high degree of similarity close to 1. This finding suggests that the model effectively learns a latent representation of the normal TFR, enabling the generation of realistic TFRs.

5) Encoder Training: After training the mapping from the real TFR to the latent space and the inverse mapping from the latent space back to the real TFR, the corresponding latent encoding for a given query input can be obtained using the encoder. If the input falls within the range of the training data, the model can identify visually similar normal TFRs. The average SSIM value between the reconstructed TFR and the original TFR is calculated as 0.84 using the proposed method. This value, close to 1, indicates that the model can accurately learn a latent representation of the normal TFR for effective reconstruction.

6) Ensembled Training: During the training process of AE-AnoWGAN, we adopt a selective approach where only one generator–discriminator pair is updated in each training iteration, instead of updating all generators and discriminators simultaneously. Specifically, a generator and a discriminator are randomly chosen, and the loss is computed using random batches of training data. It is important to note that AE-AnoWGAN does not require IJ times the training time of the basic model; in fact, it is significantly faster. This efficiency is achieved by updating the generator once every I iterations on average, with a similar approach for the discriminator. In practical implementations, using small values of I and J ($e.g., I = J = 3$) often leads to substantial performance improvements.

7) Comparison Experiment: In order to demonstrate the effectiveness of the proposed method, various anomaly detection methods are employed to analyze the same data set for comparison. These include the GAN-based anomaly detection method, GANomaly, as well as other methods, such as FastFlow, PADIM, STFPM, and reverse distillation, which are integrated with the anomalib library [46]. The corresponding ROC curve and AUC value of the analysis results are presented in Fig. 5.

Notably, the AUC value achieved by AE-AnoWGAN on the PU bearing data set reaches 0.98, surpassing other

TABLE III
TIME-CONSUMING COMPARISON OF ANOMALY DETECTION METHODS

Anomaly Detection Methods	Duration
FastFlow	13min 35s
PADIM	11min 1s
STFPM	12min 47s
Reverse Distillation	10min 18s
GANomaly	12min 12s
AE-AnoWGAN	58.79s

state-of-the-art methods for bearing anomaly detection. The exceptional performance can be attributed to the advanced integrated GAN framework and the sophisticated reconstruction process facilitated by the Encoder. These components significantly enhance the accuracy of anomaly detection compared to other methods.

Although these anomaly detection methods exhibit good performance, their computational efficiency in practical applications is low. In contrast, the AE-AnoWGAN technology significantly enhances speed by replacing the iterative process with a learning mapping from the image to the latent space. Table III presents the time-consuming comparison results of different anomaly detection methods using the RTX3090 graphics card, based on the evaluation of 4899 TFRs in the test set. Remarkably, compared to the best performing anomaly detection method, Reverse Distillation, AE-AnoWGAN achieves a reduction in running time of approximately 90%. This improvement is critical and highly valuable in industrial settings that demand real-time anomaly detection capabilities.

8) Anomalies Localization: Once AE-AnoWGAN are trained, the effectiveness of the proposed method for anomaly localization is verified by analyzing the test data set. The TFRs in the test set are used as inputs. Subsequently, the model generates a reconstructed TFR representing the normal signals, enabling accurate pixel-level localization of anomalies by comparing the two TFRs.

As shown in Fig. 6, the TFR enclosed in the red frame represents the abnormal input, the TFR enclosed in the yellow frame represents the generated TFR, and the TFR

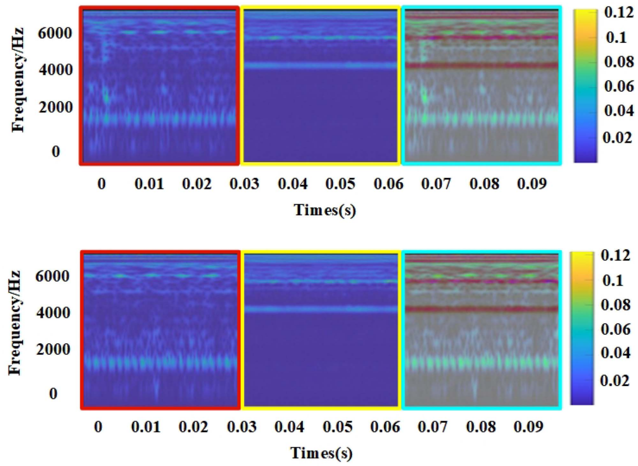

(a)

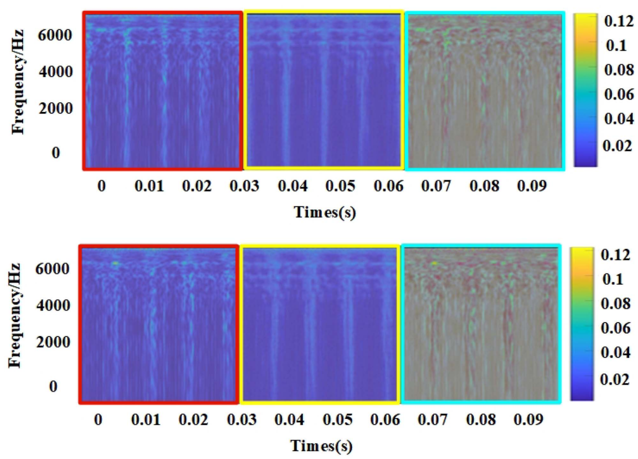

(b)

Fig. 6. Pixel-level anomaly localization of (a) abnormal input TFR and (b) normal input TFR. The TFR enclosed in the red, yellow, and blue frames represents the input abnormal TFR, the generated TFR, and the result of anomaly location, respectively. This approach enables the precise localization of anomalies at the pixel level.

enclosed in the blue frame illustrates the result of anomaly localization. The red portion within the blue frame indicates the location mark of the anomaly. Fig. 6(a), displays the result of the abnormal input TFR, while Fig. 6(b) shows the outcome of the normal input TFR. Notably, the anomaly location in the normal TFR is almost negligible, whereas the anomaly location in the abnormal TFR is significantly more prominent. This observation demonstrates the model's capability to distinguish between normal and abnormal TFRs, thereby effectively implementing anomaly localization.

9) Differentiate Abnormalities: Initially, the test set of the PU bearing data set is utilized as input to generate the TFRs. Subsequently, the proposed method is employed to calculate the anomaly scores for all TFRs within the test set. The test set is divided into two parts for further analysis. The first half is used to establish the threshold for anomaly scores. In the second half, any TFRs with anomaly scores surpassing the threshold are classified as anomalous. Fig. 7 provides a visual representation of the partitioning between abnormal and normal TFRs.

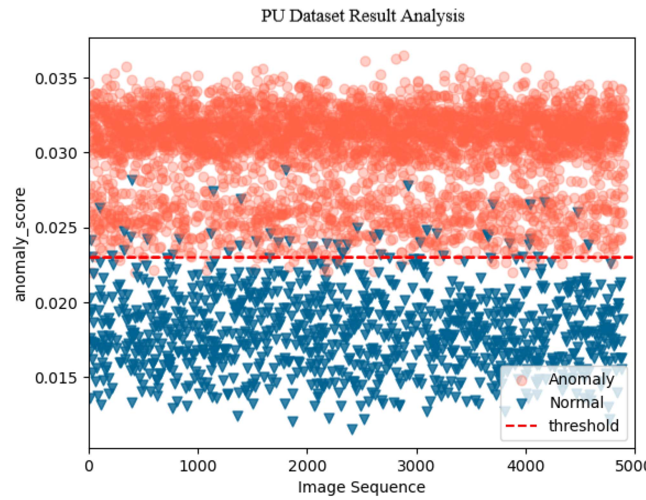

Fig. 7. Anomaly scores of normal and abnormal TFRs are depicted in the graph. The threshold of the anomaly score is indicated by a dotted line. TFR samples with anomaly scores exceeding the threshold are classified as abnormal.

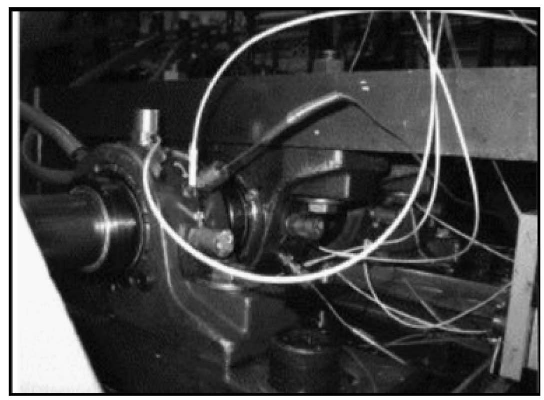

(a)

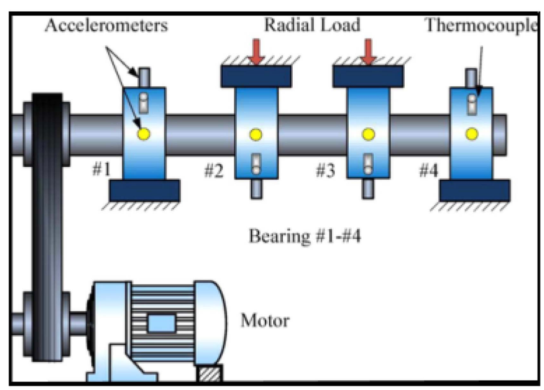

(b)

Fig. 8. (a) Test rig of the IMS bearing data set. (b) Structural diagram of the IMS test bench, including the motor, four bearings, accelerometers, radial Load, and thermocouple.

B. Case II—IMS Bearings Data Set

1) Data Description: The experimental data set in Case II is run-to-failure data set and was generated from Prognostics Center of Excellence through prognostic data repository contributed by the intelligent maintenance system (IMS), which is called the IMS bearing data set. The IMS bearing data set

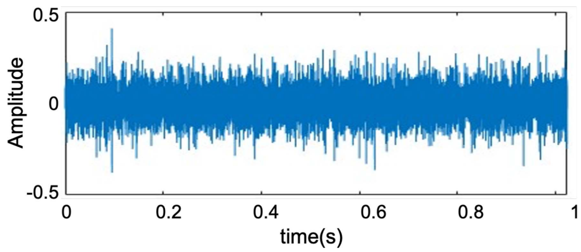

Fig. 9. Visualization of vibration signal from IMS data set.

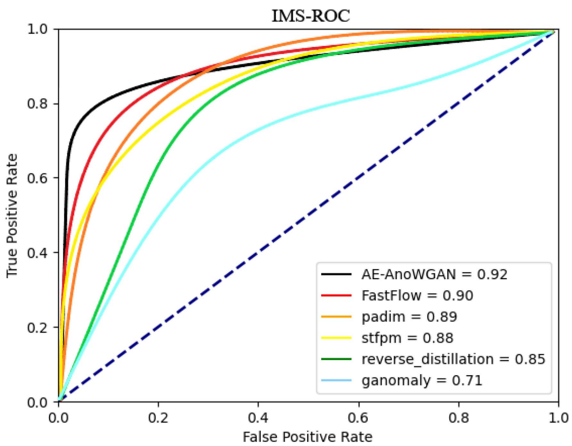

Fig. 10. ROC curve and AUC value of the analyzed results for the IMS data set are presented. It is evident that AE-AnoWGAN exhibits the highest accuracy rate among the methods evaluated.

was collected on an endurance test rig of the University of Cincinnati and was released in 2014 [47]. The experimental platform and the structural diagram of the IMS test bench are shown in Fig. 8, which has the following characteristics: 1) 4 double row bearings of type Rexnord ZA-2115; 2) stationary speed of 2000 rpm; 3) 6000 lbs load that applied onto the shaft and bearing; and 4) PCB 253B33 high-sensitivity accelerometers.

The four bearings are installed on the same shaft and are forcibly lubricated by a circulating system to regulate flow and temperature. The IMS data set includes the full life cycle data of these bearings. The visualization of the vibration signal is shown in Fig. 9. An AC motor and a friction belt are installed to keep the speed constant.

2) Data Preprocessing: The wavelet transform parameters in this study are aligned with the experimental settings of case I. Specifically, the signals from bearing 1 in both data set 1 and data set 2 are utilized. Bearing 1 in data set 1 represents a healthy state, while the outer ring of bearing 1 in data set 2 is intentionally damaged. The sampling frequency is set to 20 kHz, and each sampling has a duration of 1 s. Subsequently, the signal is divided into frames with a size of $f = 1024$. By applying the wavelet transform, the TFRs of the data set are obtained, encompassing both healthy and faulty data. In total, we obtain 4291 TFRs with a resolution of 256×256 representing the healthy state, and 1954 TFRs with the same resolution representing the inner ring fault state. The division between the training set and test set follows the same approach as the PU data set, as listed in Table I.

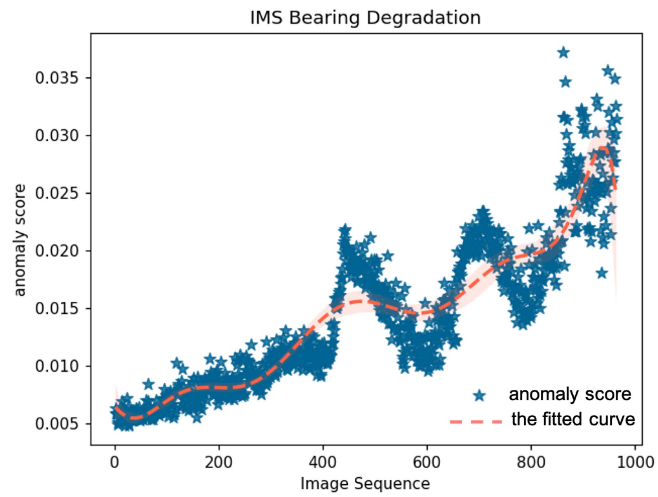

Fig. 11. As the IMS bearing data undergoes degradation, the anomaly score generated by the model continues to rise.

3) Anomaly Detection Accuracy Comparison: The experimental setup for the comparative experiment remains consistent with Case I. The corresponding ROC curve and AUC value of the IMS data set are presented in Fig. 10. Remarkably, AE-AnoWGAN achieved an AUC value of 0.92 on the IMS bearing data set, surpassing the state-of-the-art anomaly detection methods used for comparison.

4) Degradation Estimation: The proposed method utilizes the test set as input for degradation estimation. The TFRs are organized and analyzed in chronological order, and their corresponding anomaly scores are depicted in Fig. 11. Notably, the anomaly scores exhibit a clear upward trend, aligning with the continuous degradation pattern observed in bearing 1 throughout its entire lifespan. This observation indirectly demonstrates the sensitivity of the proposed method in detecting the degradation state of the operational bearing.

IV. Conclusion

This article presents AE-AnoWGAN, a novel anomaly detection method that combines autoencoders and integrated Wasserstein generative adversarial networks (WGANs). The proposed approach leverages TFRs of normal signals to train the WGAN and associated encoders, enabling the mapping of TFRs to a latent space for effective anomaly detection.

During the training process of AE-AnoWGAN, an autoencoder–discriminator pair is designed. The encoder maps TFRs to the latent space, while the pretrained generator serves as the decoder to generate reconstructed TFRs. Comparative evaluations demonstrate that our method significantly outperforms state-of-the-art approaches in terms of anomaly detection performance.

Furthermore, we conduct analyses on two distinct data sets. For the PU data set, our method exhibits excellent anomaly detection capabilities, accurately pinpointing pixel-level anomalies. In the case of the IMS degraded bearing data set, the trend of the anomaly scores aligns with the degradation patterns observed in the bearings. This correlation indirectly verifies the sensitivity and high accuracy of our anomaly scores, offering a promising tool for bearing degradation estimation.

To summarize, Generative model is a practical solution to address the few-shot problem, which is a common problem in industrial applications because the industrial systems usually work under health condition and the anomaly data set is lacking. While the training of the proposed method in this article do not need anomaly data set, which show great advantages in real engineering. In addition, our proposed method demonstrates exceptional sensitivity in detecting anomalies in abnormal bearings and effectively locates pixel-level anomalies in TFRs. Moreover, it achieves high-detection efficiency, making it suitable for real-time applications in industrial scenarios.

REFERENCES

[1] Y. Chang, J. Chen, W. Wu, T. Pan, Z. Zhou, and S. He, "Intelligent fault quantitative identification for Industrial Internet of Things (IIoT) via a novel deep dual reinforcement learning model accompanied with insufficient samples," *IEEE Internet Things J.*, vol. 9, no. 20, pp. 19811–19822, Oct. 2022.

[2] S. Lu, J. Lu, K. An, X. Wang, and Q. He, "Edge computing on IoT for machine signal processing and fault diagnosis: A review," *IEEE Internet Things J.*, vol. 10, no. 13, pp. 11093–11116, Jul. 2023.

[3] Y. Li, Y. Chen, K. Zhu, C. Bai, and J. Zhang, "An effective federated learning verification strategy and its applications for fault diagnosis in Industrial IoT systems," *IEEE Internet Things J.*, vol. 9, no. 18, pp. 16835–16849, Sep. 2022.

[4] B. Li and C. Zhao, "Federated zero-shot industrial fault diagnosis with cloud-shared semantic knowledge base," *IEEE Internet Things J.*, vol. 10, no. 13, pp. 11619–11630, Jul. 2023.

[5] H.-X. Hu, C. Cao, Q. Hu, Y. Zhang, and Z.-Z. Lin, "A real-time bearing fault diagnosis model based on Siamese convolutional autoencoder in Industrial Internet of Things," *IEEE Internet Things J.*, vol. 11, no. 3, pp. 3820–3831, Feb. 2024.

[6] J. Zhang, K. Zhang, Y. An, H. Luo, and S. Yin, "An integrated multitasking intelligent bearing fault diagnosis scheme based on representation learning under imbalanced sample condition," *IEEE Trans. Neural Netw. Learn. Syst.*, early access, Jan. 6, 2023, doi: 10.1109/TNNLS.2022.3232147.

[7] X. Yu, F. Dong, B. Xia, S. Yang, E. Ding, and W. Yu, "An intelligent fault diagnosis scheme for rotating machinery based on supervised domain adaptation with manifold embedding," *IEEE Internet Things J.*, vol. 10, no. 1, pp. 953–972, Jan. 2023.

[8] J. Chen, W. Hu, D. Cao, Z. Zhang, Z. Chen, and F. Blaabjerg, "A meta-learning method for electric machine bearing fault diagnosis under varying working conditions with limited data," *IEEE Trans. Ind. Informat.*, vol. 19, no. 3, pp. 2552–2564, Mar. 2023.

[9] Z. Yang, B. Xu, W. Luo, and F. Chen, "Autoencoder-based representation learning and its application in intelligent fault diagnosis: A review," *Measurement*, vol. 189, Feb. 2022, Art. no. 110460.

[10] Y. Djenouri, A. Belhadi, G. Srivastava, U. Ghosh, P. Chatterjee, and J. C.-W. Lin, "Fast and accurate deep learning framework for secure fault diagnosis in the Industrial Internet of Things," *IEEE Internet Things J.*, vol. 10, no. 4, pp. 2802–2810, Feb. 2023.

[11] Z. An, S. Li, J. Wang, and X. Jiang, "A novel bearing intelligent fault diagnosis framework under time-varying working conditions using recurrent neural network," *ISA Trans.*, vol. 100, pp. 155–170, May 2020.

[12] R. Huang, J. Li, Y. Liao, J. Chen, Z. Wang, and W. Li, "Deep adversarial capsule network for compound fault diagnosis of machinery toward multidomain generalization task," *IEEE Trans. Instrum. Meas.*, vol. 70, pp. 1–11, 2021.

[13] Z. Xu, C. K. M. Lee, Y. Lv, and J. Chan, "Ensemble capsule network with an attention mechanism for the fault diagnosis of bearings from imbalanced data samples," *Sensors*, vol. 22, no. 15, p. 5543, 2022.

[14] W. Li, H. Lan, J. Chen, K. Feng, and R. Huang, "WavCapsNet: An interpretable intelligent compound fault diagnosis method by backward tracking," *IEEE Trans. Instrum. Meas.*, vol. 72, pp. 1–11, Jun. 2023.

[15] R. Huang, J. Li, S. Wang, G. Li, and W. Li, "A robust weight-shared capsule network for intelligent machinery fault diagnosis," *IEEE Trans. Ind. Informat.*, vol. 16, no. 10, pp. 6466–6475, Oct. 2020.

[16] Q. Huang, R. Wen, Y. Han, C. Li, and Y. Zhang, "Intelligent fault identification for Industrial Internet of Things via prototype guided partial domain adaptation with momentum weight," *IEEE Internet Things J.*, vol. 10, no. 18, pp. 16381–16391, Sep. 2023.

[17] X. Liu, S. Liu, J. Xiang, and R. Sun, "A transfer learning strategy based on numerical simulation driving 1D cycle-GAN for bearing fault diagnosis," *Inf. Sci.*, vol. 642, Sep. 2023, Art. no. 119175.

[18] H. Wang, J. Zheng, and J. Xiang, "Online bearing fault diagnosis using numerical simulation models and machine learning classifications," *Rel. Eng. Syst. Safety*, vol. 234, Jun. 2023, Art. no. 109142.

[19] R. Liu, B. Yang, and A. G. Hauptmann, "Simultaneous bearing fault recognition and remaining useful life prediction using joint-loss convolutional neural network," *IEEE Trans. Ind. Informat.*, vol. 16, no. 1, pp. 87–96, Jan. 2020.

[20] A. Ding, Y. Qin, B. Wang, X. Cheng, and L. Jia, "An elastic expandable fault diagnosis method of three-phase motors using continual learning for class-added sample accumulations," *IEEE Trans. Ind. Electron.*, early access, Aug. 15, 2023, doi: 10.1109/TIE.2023.3301546.

[21] Y. Hu, R. Liu, X. Li, D. Chen, and Q. Hu, "Task-sequencing meta learning for intelligent few-shot fault diagnosis with limited data," *IEEE Trans. Ind. Informat.*, vol. 18, no. 6, pp. 3894–3904, Jun. 2022.

[22] G.-J. Qi and J. Luo, "Small data challenges in big data era: A survey of recent progress on unsupervised and semi-supervised methods," *IEEE Trans. Pattern Anal. Mach. Intell.*, vol. 44, no. 4, pp. 2168–2187, Apr. 2022.

[23] C. Shang, C.-Y. Chang, J. Liu, S. Zhao, and D. S. Roy, "FIID: Feature-based implicit irregularity detection using unsupervised learning from IoT data for homecare of elderly," *IEEE Internet Things J.*, vol. 7, no. 11, pp. 10884–10896, Nov. 2020.

[24] Y. Guo, T. Ji, Q. Wang, L. Yu, G. Min, and P. Li, "Unsupervised anomaly detection in IoT systems for smart cities," *IEEE Trans. Netw. Sci. Eng.*, vol. 7, no. 4, pp. 2231–2242, Oct.–Dec. 2020.

[25] J. Dai, J. Wang, W. Huang, J. Shi, and Z. Zhu, "Machinery health monitoring based on unsupervised feature learning via generative adversarial networks," *IEEE/ASME Trans. Mechatronics*, vol. 25, no. 5, pp. 2252–2263, Oct. 2020.

[26] T. Schlegl, P. Seeböck, S. M. Waldstein, U. Schmidt-Erfurth, and G. Langs, "Unsupervised anomaly detection with generative adversarial networks to guide marker discovery," in *Proc. 25th Int. Conf. Inf. Process. Med. Imag.*, 2017, pp. 146–157.

[27] H. Wang, J. Xu, C. Sun, R. Yan, and X. Chen, "Intelligent fault diagnosis for planetary gearbox using time-frequency representation and deep reinforcement learning," *IEEE/ASME Trans. Mechatronics*, vol. 27, no. 2, pp. 985–998, Apr. 2022.

[28] M. Arjovsky, S. Chintala, and L. Bottou, "Wasserstein generative adversarial networks," in *Proc. Int. Conf. Mach. Learn.*, 2017, pp. 214–223.

[29] I. Gulrajani, F. Ahmed, M. Arjovsky, V. Dumoulin, and A. C. Courville, "Improved training of Wasserstein gans," in *Proc. Adv. Neural Inf. Process. Syst.*, 2017, pp. 1–11.

[30] B. Neyshabur, S. Bhojanapalli, and A. Chakrabarti, "Stabilizing GAN training with multiple random projections," 2018, *arXiv:1705.07831*.

[31] S. Kawakura and R. Shibasaki, "Deep learning with AnoGAN and efficient GAN to judge agricultural harvest image data," in *Proc. Joint 9th Int. Conf. Inf., Electron. Vis. (ICIEV) 4th Int. Conf. Imag., Vis. Pattern Recognit. (icIVPR)*, 2020, pp. 1–8.

[32] Y. Wang, Y. Guo, Z. Xu, and H. Sun, "Distribution system anomaly detection based on AnoGAN embedded with cross-stitch units," in *Proc. IEEE 4th Conf. Energy Internet Energy Syst. Integr. (EI2)*, 2020, pp. 3045–3050.

[33] R. Yan, R. X. Gao, and X. Chen, "Wavelets for fault diagnosis of rotary machines: A review with applications," *Signal Process.*, vol. 96, pp. 1–15, Mar. 2014.

[34] B. Sun et al., "Small sample reliability assessment with online time-series data based on a worm WGAN learning method," *IEEE Trans. Ind. Informat.*, vol. 19, no. 2, pp. 1207–1216, Feb. 2023.

[35] D. Kim, J. Cha, S. Oh, and J. Jeong, "AnoGAN-based anomaly filtering for intelligent edge device in smart factory," in *Proc. 15th Int. Conf. Ubiquitous Inf. Manage. Commun. (IMCOM)*, 2021, pp. 1–6.

[36] T. Salimans, I. Goodfellow, W. Zaremba, V. Cheung, A. Radford, and X. Chen, "Improved techniques for training gans," in *Proc. 30th Adv. Neural Inf. Process. Syst.*, 2016, pp. 1–9.

[37] T. Liu, H. Liu, Y. Li, Z. Zhang, and S. Liu, "Efficient blind signal reconstruction with wavelet transforms regularization for educational robot infrared vision sensing," *IEEE/ASME Trans. Mechatronics*, vol. 24, no. 1, pp. 384–394, Feb. 2019.

[38] S. Akcay, A. Atapour-Abarghouei, and T. P. Breckon, "GANomaly: Semi-supervised anomaly detection via adversarial training," in *Proc. 14th Asian Conf. Comput. Vis.*, 2018, pp. 622–637.
[39] J. Yu et al., "FastFlow: Unsupervised anomaly detection and localization via 2D normalizing flows," 2021, *arXiv:2111.07677*.
[40] T. Defard, A. Setkov, A. Loesch, and R. Audigier, "Padim: A patch distribution modeling framework for anomaly detection and localization," in *Proc. Int. Conf. Pattern Recognit.*, 2021, pp. 475–489.
[41] G. Wang, S. Han, E. Ding, and D. Huang, "Student-teacher feature pyramid matching for unsupervised anomaly detection," 2021, *arXiv:2103.04257*.
[42] H. Deng and X. Li, "Anomaly detection via reverse distillation from one-class embedding," in *Proc. IEEE/CVF Conf. Comput. Vis. Pattern Recognit. (CVPR)*, 2022, pp. 9737–9746.
[43] S. Wang, D. Wang, D. Kong, J. Wang, W. Li, and S. Zhou, "Few-shot rolling bearing fault diagnosis with metric-based meta learning," *Sensors*, vol. 20, no. 22, p. 6437, 2020.
[44] D. K. Alves, R. L. A. Ribeiro, F. B. Costa, and T. O. A. Rocha, "Real-time wavelet-based grid impedance estimation method," *IEEE Trans. Ind. Electron.*, vol. 66, no. 10, pp. 8263–8265, Oct. 2019.
[45] H. Li, Q. Meng, X. Li, R. Jia, and J. Dang, "Fault identification of hydroelectric sets based on time-frequency diagram and convolutional neural network," in *Proc. IEEE 8th Int. Conf. Adv. Power Syst. Autom. Protect. (APAP)*, 2019, pp. 1447–1450.
[46] S. Akcay, D. Ameln, A. Vaidya, B. Lakshmanan, N. Ahuja, and U. Genc, "Anomalib: A deep learning library for anomaly detection," in *Proc. IEEE Int. Conf. Image Process. (ICIP)*, 2022, pp. 1706–1710.
[47] W. Gousseau, J. Antoni, F. Girardin, and J. Griffaton, "Analysis of the rolling element bearing data set of the Center for intelligent maintenance systems of the university of Cincinnati," in *Proc. 13th Int. Conf. Condit. Monit. Mach. Failure Prevent. Technol.*, 2016, pp. 1–13.

Ruonan Liu (Member, IEEE) received the B.S., M.S. and Ph.D. degrees from Xi'an Jiaotong University, Xi'an, China, in 2013, 2015, and 2019, respectively.

She was a Postdoctoral Researcher with the School of Computer Science, Carnegie Mellon University, Pittsburgh, PA, USA, in 2019. She is currently an Associate Professor with the Department of Automation, Shanghai Jiao Tong University, Shanghai, China. She is also an Alexander von Humboldt Fellow with the Institute for Automatic Control and Complex Systems, University of Duisburg-Essen, Duisburg, Germany. Her research interests include machine learning, intelligent manufacturing, and computer vision.

Dr. Liu has been awarded the 2021 Outstanding Paper Award by IEEE TRANSACTIONS ON INDUSTRIAL INFORMATICS and selected in the Young Elite Scientist Sponsorship Program by CAST in 2022.

Dong Xiao is currently pursuing the bachelor's degree in artificial intelligence with the College of Intelligence and Computing, Tianjin University, Tianjin, China.

His research interests include deep learning, computer vision, and fault diagnosis of mechanical systems.

Di Lin (Member, IEEE) received the bachelor's degree in software engineering from Sun Yat-sen University, Guangzhou, China, in 2012, and the Ph.D. degree from The Chinese University of Hong Kong, Hong Kong, in 2016.

He is currently an Associate Professor with the College of Intelligence and Computing, Tianjin University, Tianjin, China. His research interests are computer vision and machine learning.

Weidong Zhang (Senior Member, IEEE) received the B.S., M.S., and Ph.D. degrees in control science and engineering from Zhejiang University, Hangzhou, China, in 1990, 1993, and 1996, respectively.

He is currently the Director of the Engineering Research Center of Marine Automation, Shanghai Municipal Education Commission, Shanghai, China. He was as a Postdoctoral Fellow with Shanghai Jiao Tong University, Shanghai, where he was an Associate Professor in 1998, and has been a Full Professor, since 1999. From 2003 to 2004, he was an Alexander von Humboldt Fellow with the University of Stuttgart, Stuttgart, Germany. From 2013 to 2017, he was the Deputy Dean with the Department of Automation. He has authored or coauthored more than 300 papers and one book, and has been recognized as an Elsevier's Most Cited Researcher. His research interests include control theory, machine learning theory, and their applications in industry and autonomous systems.

Dr. Zhang is a recipient of National Science Fund for Distinguished Young Scholars, China.